Detection of Amyloid-β Fibrils Using Track-Etched Nanopores: Effect of Geometry and Crowding

Nathan Meyer, Nicolas Arroyo, Jean-Marc Janot, Mathilde Lepoitevin, Anna Stevenson, Imad Abrao Nemeir, Veronique Perrier, Daisy Bougard, Maxime Belondrade, Didier Cot, et al.

Detection of Aβ fibrils using track-etched nanopores: effect of geometry and crowding

Nathan Meyer[ab], Nicolas Arroyo[c], Jean-Marc Janot[a], Mathilde Lepoitevin[d], Anna Stevenson[d,e] , Imad Abrao Neimer[a], Veronique Perrier[b], Daisy Bougard[f], Maxime Belongrade[f], Didier Cot[a], Jérémy Bentin[c], Fabien Picaud[c], Joan Torrent[b], Sebastien Balme[a]*

[a] *Institut Européen des Membranes, UMR5635 UM ENCSM CNRS, Place Eugène Bataillon, 34095 Montpellier cedex 5, France.*

[b] *INM UM, CNRS, INSERM, Place Eugène Bataillon, 34095 Montpellier cedex 5, France.*

[c] *Laboratoire de Nanomédecine, Imagerie et Thérapeutique, EA4662, Université Bourgogne-Franche-Comté (UFR Sciences et Techniques), Centre Hospitalier Universitaire de Besançon, 16 route de Gray, 25030 Besançon, France*

[d] *Institut des Matériaux Poreux de Paris (IMAP), UMR 8004 CNRS, Ecole Normale Supérieure de Paris, Ecole Supérieure de Physique et de Chimie Industrielles de Paris, PSL Université, 75005 Paris, France*

[e] *School of Chemistry, University of St. Andrews, St. Andrews KY16 9ST, UK*

[f] *Pathogenesis and Control of Chronic and Emerging Infections, Univ Montpellier, INSERM, EFS, Univ Antilles, Montpellier, France*

*Corresponding Author : sebastien.balme@umontpellier.fr

Keyword : Nanopore, amyloid, track-etched, Aβ peptides, single molecule, sensor

Abstract

Several neurodegenerative diseases have been linked to proteins or peptides that are prone to aggregate in different brain regions. Aggregation of amyloid-β (Aβ) peptides are recognized as the main cause of AD progression, leading to the formation of toxic Aβ oligomers and amyloid fibrils. The molecular mechanism of Aβ aggregation is complex and still not fully understood. Nanopore technology provides a new way to obtain kinetic and morphological aspects of Aβ aggregation at single-molecule scale without labelling, by detecting the electrochemical signal of the peptides when they pass through the hole. Here, we investigate the influence of nanoscale geometry (conical and bullet-like shape) of a track-etched nanopore pore as well as the effect of molecular crowding (polyethylene glycol-functionalized pores) on Aβ fibril sensing and analysis. Various Aβ fibril samples that differed by their length were produced by sonication of fibrils obtained in the presence of epigallocatechin gallate (EGCG). The conical nanopore functionalized with PEG 5 kDa is suitable to discriminate of the fibril size from *relative current blockade*. The bullet-like shape nanopore enhances the amplitude of the current and increases the dwell time allowing to well discern the fibrils. Finally, the nanopore crowded with PEG 20 kDa enhance the relative current blockade and increase the dwell time, however, the discrimination is not improved compared to the "bullet-shape" nanopore.

1. Introduction

One central event in Alzheimer's disease (AD) is the formation of cerebral senile plaques consisting of aggregated amyloid-β (Aβ) peptides [1–3]. Their mechanism of aggregation is currently not fully understood due to the coexistence of numerous transient species at each stage of aggregation [4]. However, the Aβ peptide assembly occurs through three main steps that can be characterized by the intermediates that compose the reaction [5]. The first step corresponds to a lag phase that contains small amyloid intermediates (oligomers). Then, the second step leads to the formation of mature oligomers allowing a rapid exponential growth of their size. During this, the Aβ intermediates are highly polydispersed and small oligomers and fibrils coexist. After reaching the plateau phase of aggregation, fibrils undergo a slow maturation over time. At this step, small intermediates are almost no longer present and morphological changes in fibrils can be tertiary or quaternary in origin [6]. To fully understand the dynamic of the Aβ aggregation process, it is required to obtain the information about the kinetic and the morphology of the aggregate that is impossible presently to obtain with a single method. Therefore, an experimental technique is needed to study both aspects. The development of such technique is important to improve our knowledge of amyloid aggregation but also the treatment and the early diagnosis of AD.

The nanopore technology can detect objects at the single molecule level[7]. The classical experiments consist in recording the current perturbation during the translocation of an object under an applied voltage bias[8]. These perturbations give information about the properties of the object including volume, shape or sequence [9–11]. The first demonstration of the Aβ peptide detection by nanopore was done using α-hemolysin[12]. The latter allow discriminating the random coil vs β-sheet structure of Aβ25-35, based on the amplitude of the relative current blockade[13]. However, the main limitation of the α-hemolysin is the

small aperture where the Aβ fibrils (or large oligomers) cannot pass through generating only bumping events[14]. Compared to biological nanopores, the geometry of the solid-state ones can easily be tuned from a couple of nm to μm diameter with high or low aspect ratio (defined from the ratio length/diameter)[15]. This allows the detection of various biomacromolecules from folded to unfolded proteins to virus[16–20]. Thanks to an adjustable the pore size, the detection of protein aggregates by solid-state nanopore is currently an active field[21]. Silicium Nitride (SiN) nanopores allow the discrimination of amorphous and ordered aggregates as well as small oligonucleotide[9,22,23]. However, intrinsically disordered proteins require a surface functionalization of the silicon nitride to prevent the nanopore fouling[10]. This can be achieved by different coating of the nanopore surface by phospholipids, surfactants or PEG grafting[22,24,25]. On the other hand, the fibril detection is limited by the size of the nanopore aperture as illustrated by the bumping events reported for the Aβ aggregates detected by nanopipette[14,26]. To overcome this limitation, we proposed to use a conical nanopore obtained by the track-etched method in polymer film functionalized by PEG to prevent the fouling[27]. Using this strategy, β-lactoglobulin and Tau amyloids were detected, by their passage from the large to small aperture[28]. A similar strategy was also reported to detect α-synuclein aggregates using a nanopipette[29]. Despite a low resolution, the polymer track-etched nanopore presents numerous advantages. First, the intrinsic method of fabrication allows the nanopore being already filled with an aqueous solution after chemical etching, limiting thus the problem of the wettability. In addition, the surface modification is easy to achieve in aqueous solution and it is possible to know the surface density of the grafting[30]. Finally, the track-etched nanopores are exceptionally stable after PEG grafting and can be used for resistive pulse experiments for several

weeks[28,31]. This was also the case for the SiN functionalized with PEG incorporated in microfluidic chamber[32].

Despite the feasibility of investigating protein aggregation, the nanopore technology shows limitations to study the Aβ fibrils due to their adsorption and thus such goal is still challenging. In addition, all the previous studies were done on heterogenous samples and thus the real morphology and volume of amyloid are not controlled. This work aims to overcome this limitation by proposing an optimal nanopore to detect well-calibrated Aβ42 fibrils. Based on our previous studies[28,33], we have considered the conical track-etched nanopore as the most suitable to detect small fibrils thank to the combination of a large aperture favouring fibre trapping and the small one as sensing zone[28].

To demonstrate that, we have designed, a conical track-etched nanopores and to detect well-calibrated small fibrils of Aβ42 peptides. Then, we also ask the question about the optimal conditions to discriminate different sizes of fibrils in terms of pore geometry. We have considered two potential strategies to improve the fibril discrimination: the nanopore geometry and the crowding. Concerning the geometry the "bullet-like" shape nanopore allow reducing the detection zone compared to the conical shape nanopore. We hypothesize that this will enhance the amplitude of the current blockade and thus expect an improvement of the discrimination of fibre size. On the other hand, several previous investigations obtained using crowded nanopores are consistent with an essential role of auxiliary macromolecules to improve nanopore detection capabilities[29,34]. According to that, here we have considered crowding the tip aperture of the nanopore. In this strategy, we hypothesize that the crowding will increase the dwell time of fibre inside the nanopore

but also amplitude of the current blockade. Thus, we could also expect to better discriminate the fibril with different sizes than conical nanopore.

To verify our two hypotheses and finally propose a suitable nanopore geometry to detect and discriminated Aβ42 fibrils fibril, we designed track-etched nanopores, from conical to bullet-like shapes. The nanopore were functionalized with PEG 5 kDa and 20 kDa to induce a crowded environment. In parallel, we produced and characterize by microscopy well-calibrated Aβ42 fibrils with different sizes. Then, we detect of calibrated Aβ42 fibres using the different nanopores (conical, "bullet-like" shape and crowded). For each nanopore, the experimental result was discussed in order to compare the different strategy. Finally, molecular dynamics simulations have been also conducted to understand at the nanoscale the translocation of the fibrils in a crowded nanopore.

2. Materials and methods

2.1. Nanopore design

Single polymer nanopore was obtained by the track-etched method. The single tracks were produced by Xe irradiation (8.98 MeV u^{-1}) (GANIL, SME line, Caen, France) of polyethylene terephthalate (PET) film (thickness 13 μm or 6 μm, biaxial orientation, Goodfellow).

The conical nanopores were obtained as previously reported[35,36]. First, the tracks were activated by UV exposition 12 h per side (Fisherbioblock; VL215.MC, λ=312 nm). Then, the chemical etching was performed under unsymmetrical condition (etchant solution 9 M NaOH and stop solution 1 M KCl and 1 M of acetic acid) using the electrostopping method (1 V). The opening of the pores was monitored using an e-one amplifier or EPC 10 Heka amplifier (Element, Italy and Heka electronic, Germany). After nanopore opening, the tip

radius r was deduced from the conductance G (measured from−100 mV to 100 mV) with NaCl solution at different concentrations, assuming bulk-like ionic conductivity inside the nanopores using Equation (1).

$$G = \frac{\kappa \pi r R}{L} \qquad (1)$$

where κ is the conductivity of the solution, L the nanopore length and R the radius of the base side. The latter is obtained from the SEM image performed on multipore membranes opened under strictly the same conditions (see Figure SI-2).

The single bullet shape nanopore was obtained following the method previously reported[37,38]. Briefly, only one side of the tracked film is activated by UV for 26 h (Fisherbioblock; VL215.MC, λ=312 nm). Then, the chemical etching was performed under symmetrical conditions with NaOH 6M and Dowfax2A1(EZkem, USA) 0.05% v/v at 60°C for 8 min. At the end of the etching process, the nanopore was washed in several pure water (18.2 MOhm) baths.

The scanning electron microscope (SEM) images were performed on multipore membranes (10^8 pores/cm²), using a Thermo Scientific Quattro ESEM, at high vacuum at 10 kV and 46 pA or Hitachi S-4800.

2.2. Nanopore fonctionalization

The pores were functionalized with polyethylene glycol amine (PEG-NH_2) to reduce the fouling or to crowd the sensing zone. To do so, the nanopores were immersed overnight in a solution of PEG-NH_2 5kD for pores 1 & 2 (or PEG-NH_2 20kD for pore 3), MES 0.1 M and EDC 50 mM in KCl 0.1M. The success of the functionalization was evidenced by current-voltage measurements (See Figure SI-1).

2.3. Production of Aβ42 fibrils

154 2.3.1. Aβ42 fibril assembly

155 Synthetic human Aβ42 peptides were purchased from the ERI Amyloid Laboratory
156 LLC. Aβ peptides were dissolved at a concentration of 8.5 mg mL^{-1} in a solution of
157 guanidine thiocyanate (Sigma-Aldrich) at 6.8 M. Then, the solution was sonicated for 5
158 min at 52°C and ultrapure water was added to reach a final concentration of 5 mg mL^{-1} of
159 Aβ peptides and 4 M of guanidine thiocyanate. The solution was centrifuged at 10000×g
160 for 6 min at 4°C and the supernatant was collected and filtered (polyvinylidene fluoride
161 (PVDF); 0.45 µm). Then, the supernatant was injected into a Superdex® 75 Increase
162 10/300 GL column (GE Heathcare Life Science) equilibrated with a solution of 10 mM
163 sodium phosphate buffer (pH 7.4). A flow of 0.5 mL min^{-1} was used to collect the peak
164 corresponding to monomeric Aβ42. After the purification, the concentration of peptides
165 was determined with a NanoDrop™ 8,000 spectrophotometer (Thermo Scientific). Finally,
166 monomeric Aβ42 peptides were aliquoted and stored at −80°C until using.

167 The Aβ42 fibrils were obtained as follow. The stock solution was diluted to reach 30 µM
168 and were exposed to 25 µM of EGCG or the vehicle alone (0.05% DMSO, v=v) in a 10 mM
169 sodium phosphate buffer at pH 7.4. Peptide solutions, final volume of 600 µL, were let to
170 aggregate in low-binding Eppendorf with 30 µM Epigallocatechin Gallate (EGCG) (1:1)
171 or the vehicle alone (1% dimethyl sulfoxide, DMSO). Tubes were arranged vertically at
172 25°C without shaking (quiescent state). Thioflavin T (ThT) binding assay was used to
173 monitor the fibril formation. 20 µl of Aβ42 solution aliquots were withdrawn and mixed
174 with 14 µl of glycine-sodium hydroxide buffer (142 mM at pH 8.3) and 6 µl of ThT at 100
175 µM. The mix was placed into a 96-well plate of black polystyrene with clear bottoms and
176 a polyethylene glycol coating (Thermofisher Scientific). The fibrils formation was

monitored by following fluorescence of ThT (λ_{ex}=445 nm and λ_{em}=485 nm) with a Fluoroskan Ascent™ microplate fluorimeter (Thermofisher Scientific). Aggregation curves were generated with Matlab software (Matlab R2020a), and each kinetic trace was fitted independently using the curve fitting tools.

2.3.2. Fragmentation of Aβ42 fibrils

The fragmentation of the Aβ42 fibrils harvested at the plateau phase (see fig 1A and figSI-5) were performed at a concentration of 15 µM in 10 mM PBS by sonication at different energies either using a wet bench sonicator 34 W (Branson Ultrasonic model 200) for different times from 5 min to 45 min or a cup-horn sonicator with a power of 300 W in presence of two beads (to enhance sonication process) for 15 s or 60 s. After sonication, the samples were frozen and stocked at -80°C.

2.3.3. Transmission electron microscopy (TEM) - characterization

Samples of Aβ42 fibrils were deposited onto Formvar carbon-coated grids, negatively stained with freshly filtered 2% uranyl acetate, dried. The TEM images were performed using a JEOL 1400 electron microscope at an accelerating voltage of 80 kV. The measurements of the fibrils length and diameter were performed using ImageJ software and analysed with matlab software.

2.3.4. Aβ42 Fibers detection using nanopore

The Aβ42 fibrils were detected using the resistive pulse method. To do so, the single nanopore was mounted between two Teflon chambers containing electrolyte solutions. PBS 1X at pH 7.2 or NaCl 1M PBS, pH 7.2 was used. Electrical measurement was performed using a patch-clamp amplifier (EPC10 HEKA electronics, Lambrecht, Germany). The current was measured by electrode Ag/AgCl. For all the experiments, the

ground was placed in the chamber containing the Aβ42 fibrils (concentration 50 nM or 100 nM monomers). A positive voltage is applied on the working electrode, placed to the opposite reservoir. The data was acquired with a frequency rate of 20 kHz or 40 kHz or 100 kHz. A Bessel filter of 10 kHz was used during the recording. The data analysis was performed using a custom-made LabView software PeakNano Tools. Briefly, a Savitzky–Golay filter order 1 was used to correct the base line fluctuations. The detection of events was performed using a threshold of 4σ (σ being the standard deviation to the baseline signal). Each event was characterized by the relative current blockade ($\Delta I/I_0$), the dwell time (Δt), the slopes both at the beginning and the end of the blockade. The parameters of the current blockade were then analysed using Matlab software with custom scripts. Statistical comparisons of the Δt and $\Delta I/I_0$ were performed using t-test or welch-test for the samples with no equal variance. A probability level (p value) of 0.05 was chosen for statistical significance.

2.4. Molecular dynamics simulations

To model the resistive pulse measurements, we used classical all-atom MD simulations in the NAMD.2.12 package framework[39] with CHARMM36 force-field parameters[40].The water (described with the TIP3P model) box was chosen as large enough to prevent any interaction between each periodic cell. KCl ions (at a concentration of 1 M) were used to reproduce the experimental environment. We worked during the simulations in the NPT ensemble where temperature (300K via Langevin dynamics method[41]) and pressure (1 atm via Langevin piston method[42]) were kept constant. To take into account the long-range electrostatic forces the classical particle mesh Ewald (PME) method[43] with a grid spacing

of 1.2 Å, and a fourth-order spline interpolation was used. The integration time step was equal to 1 fs.

2.4.1. Description of the conical nanopore.

Our conical nanopore was described in previous papers[30,44] . Its dimension (R_{tip} = 3 nm, R_{base} = 3.5 nm, length=14.8 nm) was obtained through the association of several carbon nanotube sections of different radii. The chemical structure of PET nanopore as used in the experiments was modelled by replacing one third of the carbon atoms constituting the nanopore by oxygen atoms. Then partial charges were imposed to carbon (positive) and oxygen (negative) atoms while keeping global neutrality of the nanopore. According to the experimental functionalization 30 hydroxyl functions (0.10 M) were then randomly functionalized to carbon atoms and three (twenty-four) PEG 5 kDa (3 kDa) were added as in the experiments to model the conical (bullet shape) nanopore. Finally, the functionalized nanopore was solvated and attached to 2 solvated and ionized reservoirs (dimensions equal to 133*133*68 A^3). The complete system dimensions are 133*133*285 $Å^3$, for a total of around 350.000 atoms. The optimization of the systems followed three successive procedures. First, we minimized the energy of the total system at 0 K. Then, the system was progressively thermalized to a temperature equal to 300 K. Finally, the system evolved in the NPT ensemble, and physical observables were calculated using time averages. During all simulations, every atom constituting the conical nanopore wall was kept fixed. This system was relaxed for 100 ns, allowing for PEG to relax around the surface of the nanopore. To determine the ionic currents, various electric fields were applied using simulations in the NVT ensemble. The determination of the ionic current values was performed according to the procedure described previously.

245 2.4.2. Description of the simulated amyloids.

246 We studied the behaviour of two different structures: 2NAO [50] (~2000 atoms) and
247 5OQV[45] (~3000 atoms), two dual subunit amyloid fibril structures translocating through
248 the two previously described nanopores. Our objective is to study the role of PEG density
249 (crowding) on the current perturbation inside the nanopore. The translocation of these big
250 amyloid structures (both close to the tip dimensions) will allow us to understand the
251 dynamic of PEG during such protein displacement in a crowded environment. For each
252 simulation run, the already relaxed protein (for at least 5 ns) was placed at the entrance of
253 each functionalized nanopores and let diffusing inside the conical nanopore under an
254 electric field equal to 2 V.

255 3. Results and discussion.

256 3.1. Nanopore and amyloid characterization

257 3.1.1. Nanopore characterization

258 Two methods, electrostopping and surfactant controlled, were used to produce
259 unsymmetrical nanopore, leading to conical and bullet-shaped pores respectively.
260 Electrostopping was used to obtain conical-shape nanopore. The size of the nanopore was
261 determined from the conductance measurement and SEM analysis (Figures SI-1 & SI-2).
262 After etching, the nanopores were coated with PEG to prevent current rectification and
263 protein adsorption[22,28]. Two conical nanopores were obtained. The first one (noted pore 1,
264 d=40±2.5 nm, D=540 ±90 nm, and 6 µm thick) was functionalized with PEG 5 kDa (Table
265 SI-1). The other one (noted pore 3, d=28±2 nm D=635 ± 115 nm with a thickness of 13
266 µm) was functionalized with PEG 20 kDa (Table 1 in SI). The success of the nanopore
267 functionalization is directly characterized by a decrease of the current rectification as well

as the nanopore conductance due to the grafting on carboxylate ending moieties by uncharged PEG chains at the surface, as previously demonstrated[30](Figure SI-1).

The bullet-like shape nanopore was obtained using surfactants. The current-voltage dependences of the nanopore before and after PEG are reported on the SI-1. After the etching the pore exhibits a base diameter of 379 ±9 nm and a tip diameter of 78 ± 4 nm) (noted pore 2). The functionalization is characterized by a decrease of the conductance at NaCl 0.5M and the loss of ionic current rectification (Figure SI-1b).

3.1.2. Aβ42 Fibrils characterization

To validate the fibrils detection capacities of our nanopore sensing, we have to obtain well-defined Aβ42 fibrils with different sizes as standard. To produce such fibrils, we first aggregated Aβ42 monomers until reaching a plateau (black curve figure 1A) and then sonicate the fibrils. Contrary to our expectations, the sonication did not allow the fragmentation of the fibrils (Figure SI-3). It is well known that numerous molecules can interact with Aβ42 peptides and therefore modulate their assembly in terms of kinetic and structure. Among them, EGCG is a polyphenol that slow down the aggregation (Figure 1A). Indeed, without EGCG, the plateau of the Aβ42 aggregation is reached after 200 hours while in presence of EGCG, it is reached after more than 400 hours. The TEM image shows that in presence of the EGCG, the fibrils are quite long (up to several microns, figure 1B) and are not self-associated in large clumps as observed for fibrils formed by pure Aβ42 peptides (Fig SI-3). We hypothesized that this structure could be related to a greater fragility compared to Aβ42 fibrils without EGCG. Therefore, EGCG could make the fibril breakable by sonication. The fibrils formed in presence of EGCG harvested at the plateau phase were sonicated using a classical wet bench sonicator (34 W) for 5 and 45 min. After

sonication, fibrils exhibit the rod-like shape (Figures 1C and SI-4) with a diameter centred at about 20 nm regardless the sonication time. The length of the fibrils is found to be centred at 247 nm, and 151 nm for the sample sonicated for 5 and 45 min respectively (Figures 1D, E and SI-4). We notice few aggregates composed by fibrils especially for the sample sonicated 5 min.

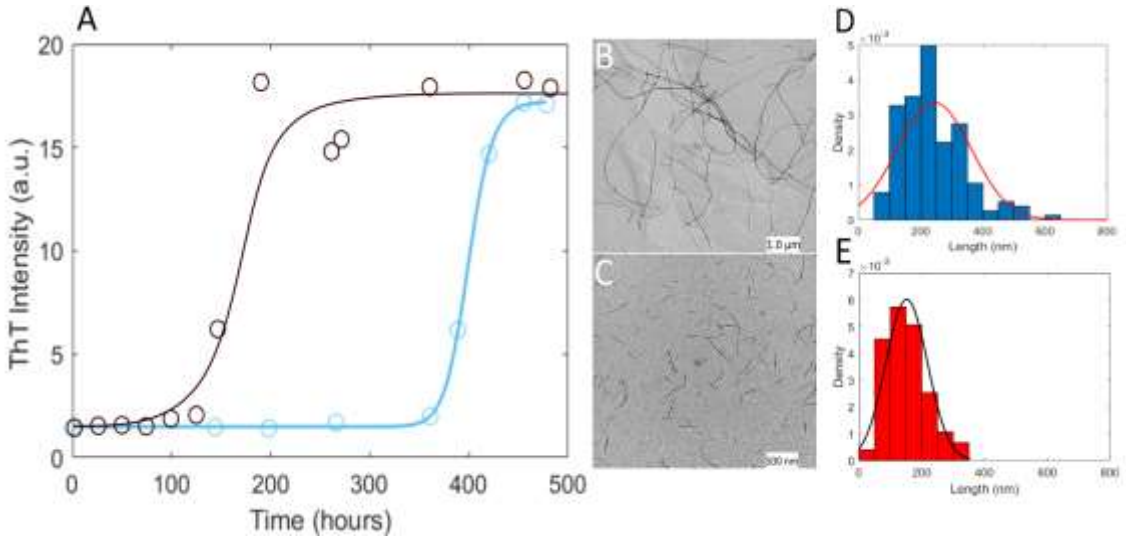

Figure 1 A) Kinetic of Aβ 42 assembly in absence (black) or in presence of EGCG (cyan). TEM images of the fibrils containing EGCG harvested in plateau phase (cyan curve) before B) and after C) 45 min of sonication by wet bench sonicator. Distribution of the fibrils length sonicated by wet bench sonicator D) 5 min (centred value of length = 247 nm, n = 153 – see also SI-4) and E) 45 min by wet bench sonicator (centred value of length = 151 nm, n = 150).

3.2. Fibrils detection using conical nanopore

We detected the sonicated fibrils using the conical nanopore (d= 36±2.5 nm and D = 540 ±90 nm) coated with PEG 5 kDa to reduce the fouling from Aβ fibrils. Under this coating and with respect to the Flory diameter[44] of PEG under good solvent conditions (5.9 nm),

we can assume that the nanopore is not under crowded condition. Usually, the detection of amyloid is performed from the base to the tip side of the nanopore to decrease the energy barrier of entrance as previously reported for β-lactoglobulin and tau[33,46]. According to that, the first set of experiments was performed in this classical method as previously reported. Typically, the Aβ42 fibrils were added on the base side to reach a final concentration of 1 μM (equivalent monomers). A positive bias (2 V) was then applied to the trans-chamber (Figure 2A). Interestingly, trapping events were observed with the sample sonicated 5 min. We observed a continuous current decrease when the sample sonicated 5 min was added (Figure SI-6). Likely due to fouling, it hinders the translocation of amyloid through the pore. To overcome this problem, we attempted to detect the fibrils from the tip to the base side of the nanopore (See figure 2A). In this case, we observed the current blockades as shown in the current traces reported on figure 2B. The event rates were 0.01, and 0.04 events s^{-1} for the sample sonicated 5, and 45 min respectively. This is consistent with the larger fibrils obtained after 5 min of sonication than after 45 min. These large fibrils are thus less concentrated (at equivalent monomer concentration) and have a slower diffusion coefficient. Regardless the sonication time, we observe that the slope of the blockade beginning, corresponding to the fibril entrance is lower but similar (same order of magnitude) that the slope at the blockade ending (Figure SI-7).

We report in figure 2C the event maps and distributions of the relative current blockade. As commonly observed for conical nanopores,[47] the dwell time distribution ranges from 0.1 ms to s scale. The scale of the dwell time and the correlation of the capture rate with the sonication time confirm that the current blockade is due to the translocation of the fibrils and not bumping. Interestingly, we can observe that the distribution of the $\Delta I_{max}/I_0$ depends

on the sonication time (Figures 2C & SI-8). Indeed, the distributions are centred at 0.008, and 0.004 for the sample sonicated 5, and 45 min respectively. This result is consistent with TEM analysis of the fibrils distribution size. In that case, the $\Delta I_{max}/I_0$ depends on the fibrils length and thus on their volume. The statistical test shows that only the $\Delta I_{max}/I_0$ is significant (Pvalue <0.05) to discriminate the two samples (Figure SI-8).

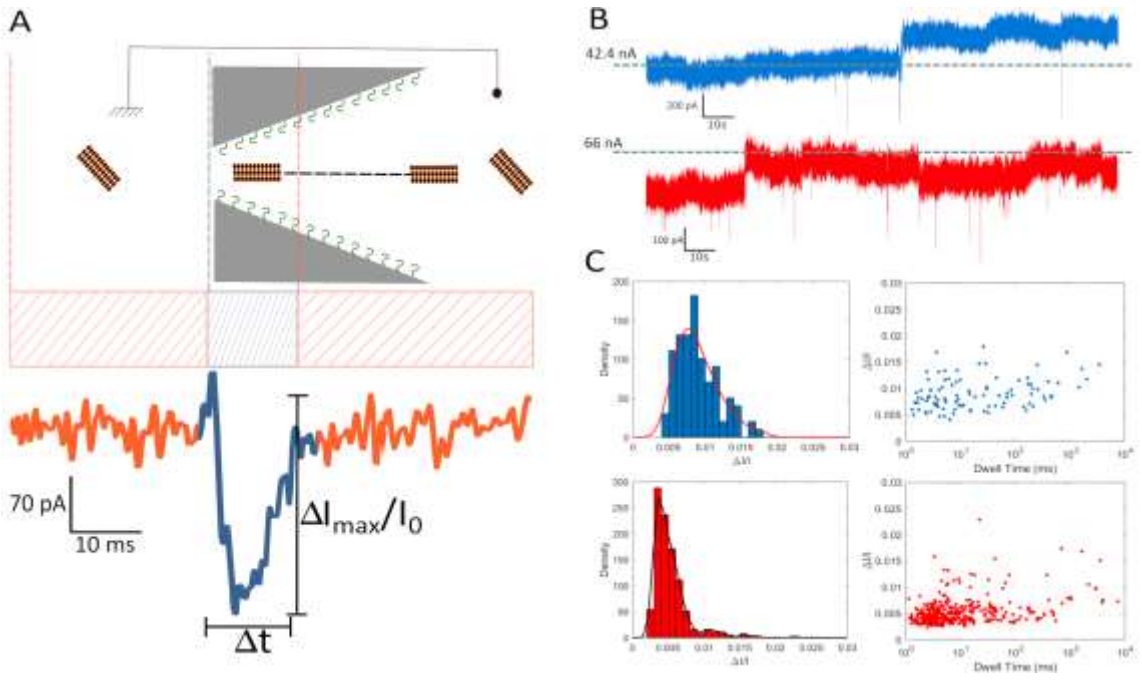

Figure 2 A) Top, sketch the fibril translocation in the large conical pore (pore 1) from tip to base in NaCl 1M (containing PBS 1X, pH 7.2) at 2 V. Bottom, zoom of a current blockade with different colours representing the fibril outside (orange) and inside (blue) the sensing zone. The maximum blockade amplitude ($\Delta I_{max}/I_0$) as well the duration of the event (Δt) are illustrated. B) The current trace recording for the sample sonicated 5 min (blue) and 45 min (red). C) Top left, distribution of the $\Delta I_{max}/I_0$ of the sample sonicated 5 min (centred $\Delta I_{max}/I_0$ value = 0.008, n = 99). Top right, scatter plot of the $\Delta I_{max}/I_0$ versus the dwell Time of the sample sonicated 5 min. Bottom left, distribution of $\Delta I_{max}/I_0$ of the

346 sample sonicated 45 min (centred $\Delta I_{max}/I_0$ value = 0.004, n = 368). Bottom right, scatter
347 plot of the dwell time versus the $\Delta I_{max}/I_0$ of the sample sonicated 45 min.

348 3.3. Fibril detection using "bullet-like" nanopore

349 We then studied whether "bullet-like" shape nanopores, which present a larger angle in
350 the tip side, improves the resolution of the fibril detection. The dimensions of the "bullet-
351 like" shape nanopore have been calibrated to obtain a tip diameter of about 78 nm and a
352 base of about 379 nm (pore 2) (Figure 3A & SI-1, 2). The pore was also coated with PEG
353 5 kD. The sonicated Aβ42 was added to the base side to reach final concentration of 50 nM
354 and 100nM (of monomers) for the sample sonicated 5 min and 45 min respectively
355 (equivalent monomer). A potential bias of 1 V was applied in the trans-chamber. In figure
356 3B are reported examples of the current traces where current blockades can be observed.
357 Firstly, the event rates were found to be 0.08, and 0.25, events s^{-1} for the sample sonicated
358 5 min and 45 min respectively. This is consistent with the difference of both aggregate size,
359 concentration of fibrils. Contrary to the conical nanopore, we observe a dissymmetry of the
360 blockade event shape. The right side of the blockade, which corresponds to the fibrils exit
361 of the nanopore, has a sharper slope compared to the left one (see figures 3A and SI-9).
362 Both the capture rate and the blockade shape evidence that the events are due to the
363 translocation of the fibrils. In figure 3C, the events map and the distribution of the relative
364 current blockades are plotted. First, we observe that for the Aβ fibrils sonicated 5 min
365 (centred to 670 ms), the dwell time is significantly longer than the one sonicated 45 min
366 (centred to 482 ms), (Figure SI-10). The centre of the $\Delta I_{max}/I_0$ is found at 0.030, and 0.017
367 for the sample sonicated 5 and 45 min, respectively (Figures 3C and SI-10). These results
368 are consistent with the TEM and the results from the conical nanopore (pore 1). However,

we can notice that the value of $\Delta I_{max}/I_0$ obtained with the bullet-like shape nanopore are one order of magnitude higher than the one obtained with the conical shape nanopore (pore 1) despite a tip radius twice larger. This can be easily explained by the morphology of the nanopore. Indeed, the length detection zone of the bullet-shape nanopore is smaller than for the conical one due to the larger angle. Compared to the conical nanopore, we notice that both $\Delta I_{max}/I_0$ and dwell time are significantly different to discriminate the two samples (Figure SI-10). In addition, using the bullet-like shape pore, we observe trapping events (Figure SI-9) for the sample sonicated 5 min. This was not observed for the sample sonicated 45 min. A possible explanation could be that after 45 min of sonication time, there is no residual large size fibrillar bundles in the solution as confirmed by the TEM analysis.

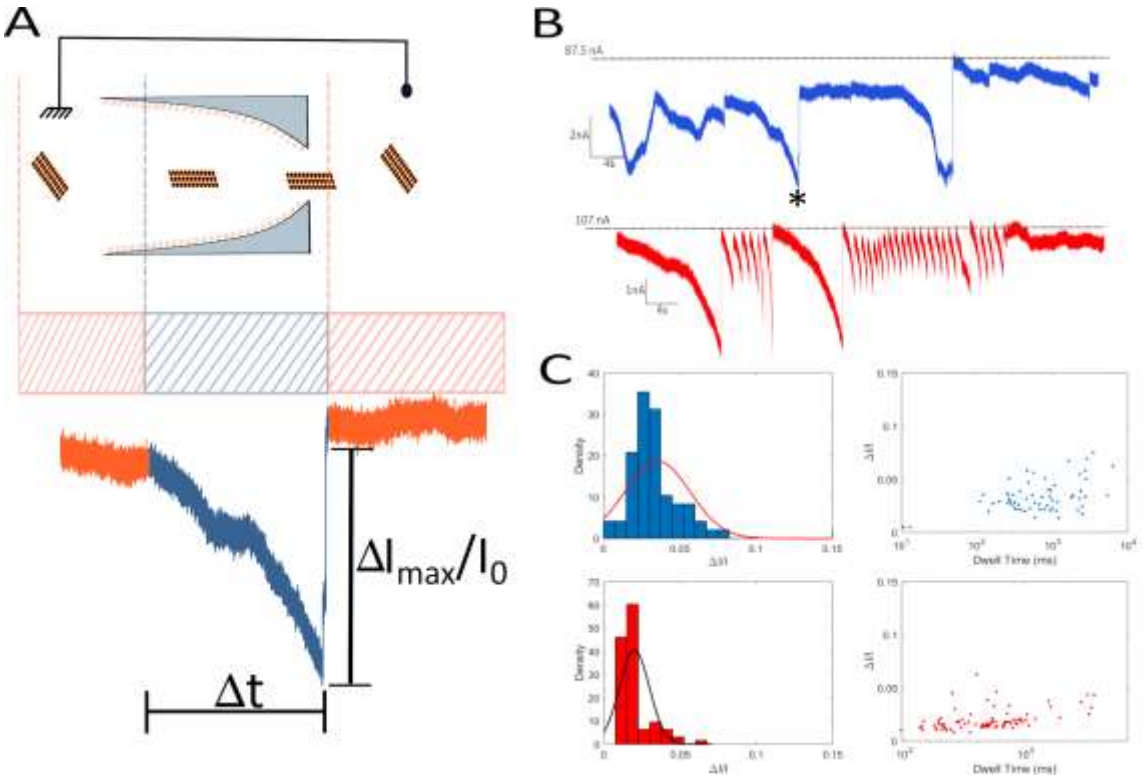

Figure 3 A) Top, sketch of Aβ42 fibril translocation into a bullet shape nanopore (pore 2) from base to tip in NaCl 1M (containing PBS 1X, pH 7.2) at 1 V. Bottom, zoom of a current

blockade with different colours representing the fibril outside (orange) and inside (blue) the sensing zone. The maximum blockade amplitude ($\Delta I_{max}/I_0$) as well the duration of the event (Δt) are illustrated. B) Current traces recording for the sample sonicated 5 min (blue) and 45 min (red). C) Top left, distribution of the $\Delta I_{max}/I_0$ for the sample sonicated 5 min (0.030, n = 64). Top right, scatter plot representing the $\Delta I_{max}/I_0$ versus the dwell time for the sample sonicated 5 min. Bottom left, distribution of $\Delta I_{max}/I_0$ of the sample sonicated 45 min (0.017, n = 84). Bottom right, scatter plot representing the dwell time versus the $\Delta I_{max}/I_0$ of the sample sonicated 45 min.

3.4. Fibril detection under crowded nanopore

In a recent work, it has been demonstrated that the crowding of one side of the nanopore enhance the detection of α-synuclein fibrils detection [29]. On the basis of this previous study and the present results, we have generated a localized crowding by grafting of long PEG chains inside the nanopore. To do so, we have opened a conical shape nanopore (pore 3, d= 28±1 nm and D= 630±110 nm). After its functionalization with PEG-NH2 20 kDa, the measured diameter of the nanopore is about 2 nm, which is in good agreement with the Flory radius in good solvent (13.75 nm) (SI-1, 2 and table 1). Thus, we can reasonably consider that the detection zone is crowded. Using this, we expect to increase the dwell time and the relative current blockade value. To illustrate this assumption, we performed molecular dynamic simulations. Because all-atom simulation does not allow to model such as of the experimental nanopore and Aβ fibril, we have used a smaller nanopore (r= 3 nm, R=3.5 nm), functionalized with PEG 5 kDa, and simulated the crowding by tuning PEG density inside the nanopore (Figure SI-11). Two different sizes of amyloid structures were used to understand the influence and role of both nanopores. For both amyloid structures,

406 we observe complete translocations under the 2 V electrical field in the low PEG density
407 nanopore. The translocation time requires around 60 ns for 5OQV (Figure 4A) and 30 ns
408 for 2NAO (Figure 4B). For the high PEG density pore, such complete translocations take
409 much more time and have not been observed within a reasonable simulated time (blue
410 curves in Figure 4). Nevertheless, in both cases we were able to analyse the behaviour of
411 the amyloid and more specifically calculate their speed inside the nanopore.
412

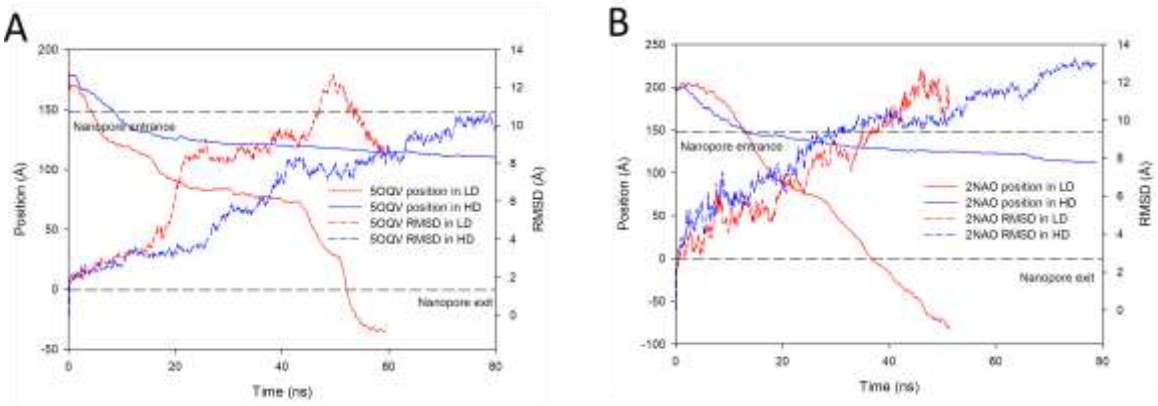

413

414 Figure 4 : Position of protein centre of mass (full line) and protein RMSD (dotted line)
415 over time. Low PEG density nanopore simulations are shown in red while high PEG
416 density nanopore is in blue. The leftmost graph represents 5OQV translocation whereas
417 rightmost graph shows 2NAO.

418

419 Plotting the position of the protein over the simulation time shows quite similar
420 behaviours for the two amyloid structures. We can, however, well distinguish the nanopore
421 type that have been crossed. In the low PEG density nanopore, we observe two regimes.
422 The first one depicts free diffusion of the amyloid through the pore while the second one
423 is characterized by the slowing down of the amyloids that have to interact strongly with

424 the crossed media (nanopore + PEG) to find its way. This behaviour is especially clearer
425 for large amyloid (5OQV) compared to smaller one (2NAO). In the first regime, the
426 amyloid is slowing down just after its entering in the pore (~8 ns), then it undergoes heavy
427 modification of its conformation (as RMSD increases from around 3 to 7.5 Å). At this point
428 the amyloid starts gaining speed again. Then, from around 20 ns we observe a second
429 plateau until 45 ns where the RMSD once again abruptly increases, freeing the protein.
430 The amyloids plunged in the high PEG density nanopore also show two distinct, but not
431 intertwined regimes. Entering the high PEG density nanopore is slightly slower than
432 entering the low PEG density one as PEG already interacts heavily right at the entrance
433 with the amyloid. We then observe a shift to a slower but constant speed for the rest of the
434 simulated time. As the amyloid is now in constant interaction with the functionalization
435 and the pore, its speed is comparable to the one in the low PEG density nanopore when the
436 amyloid slows down. Average speeds observed at the different regimes are summarized in
437 table 1.
438
439

	2NAO		5OQV	
LD nanopore	Time interval (ns)	Speed (m/s)	Time interval (ns)	Speed (m/s)
"Free" movement	3.5-18	0.77	1-6.2	0.84
	27-42	0.69	42.9-55.4	0.86
"Hindered" movement	18-27	0.28	6.2-15.5	0.18
			15.5-22.6	0.29
			22.6-42.9	0.06

HD nanopore				
Pore entrance	1.5-13	0.43	1-11.8	0.39
Inside the pore	13-77	0.05	11.8-100	0.03

Table 1: Time analysis and speed values of the two amyloids in the two different conical nanopore (LD for low PEG density and HD for high PEG density functionalization of the conical nanopore).

We also have also reported the current blockades occurring during the translocation (see SI-section Additional result of Molecular dynamic simulation). We have to notice that the MD simulation and the experimental nanopores are too far to make any conclusion about the amplitude of the current blockade. Thus, at this stage, the molecular dynamic simulation only predicts that crowding will allow increasing the amyloid dwell time inside the nanopore due to the PEG/amyloid interactions.

3.4.1. Characterization of cup horn fragments

Because we use a crowded nanopore, the experiment requires small fibrils to avoid trapping events. To do so, we performed sonication of fibrils assembled in presence of EGCG using a cup horn sonicator (300 W) during 15 s and 60 s (See FigSI-5). As expected, the fibrils are homogeneously broken with a diameter of about 10-15 nm as shown in TEM images (Figure SI-5) and length distributions centred at 114 nm and 61 nm after sonication of 15 s and 60 s respectively (Figures 5B and D).

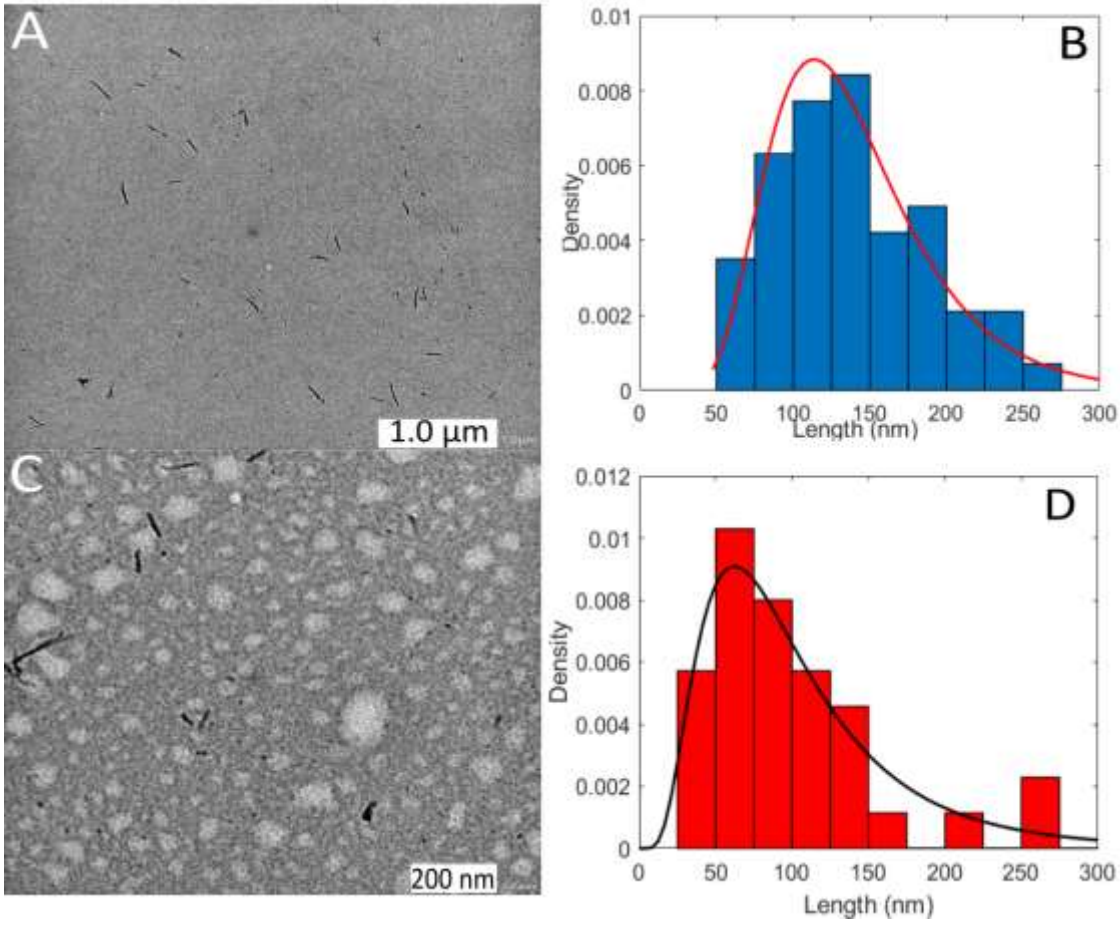

Figure 5 A) TEM image of the fibrils sonicated 15 s with a cup horn sonicator. B) length distribution of the fibrils in A (length = 114 nm, n = 57). C) TEM image of the fibrils sonicated 60 s with a cuphorn sonicator. D) length of the fibrils in C (length = 61 nm, n = 35).

3.4.2. Detection of fibrils using conical nanopore with crowded aperture

Detection of Aβ42 fibrils was done by resistive pulse experiments. Aβ42 fibrils were added in the base side (15, 75 or 150 nM) of the pore and a bias of 2 V was applied on the opposite side. As shown in the figure 6A, Aβ42 fibrils sonicated for 15 s and 60 s were analysed by recording current blockades.

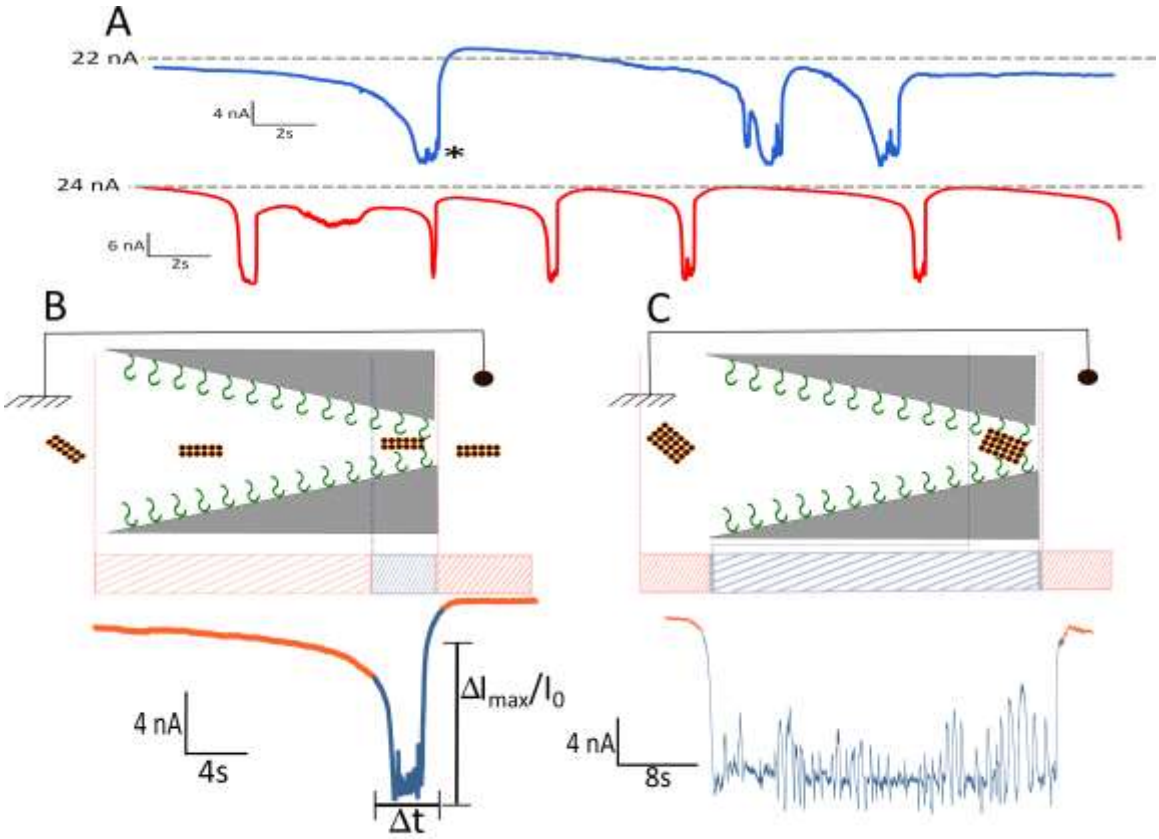

Figure 6: A) Current trace of translocation events for the samples sonicated 15 s (blue) and 60 s (red) from base to tip in PBS 1X at 1 V. B) Top, sketch of Aβ42 fibril translocation into a small conical nanopore (pore 3) in crowded condition. Bottom, zoom of a current blockade with different colours representing the fibril outside (orange) and inside (blue) the sensing zone. The maximum blockade amplitude ($\Delta I_{max}/I_0$) as well the duration of the event (Δt) are illustrated. C) Sketch of Aβ42 fibrils trapping events into a small conical nanopore (pore 3). Bottom, zoom of a trapping event with different colours representing the several steps of the trapping.

For both fibril samples, the current blockades exhibit a characteristic profile that can be divided in 4 steps, characteristic of the conical shape nanopore (Figure 6B). In the first step, the current slowly decreases during several seconds. This response could be assigned

to the reorientation of the fibril inside the nanopore to adopt a favourable conformation to translocate. Then, a larger current decrease is observed corresponding to the entrance of the fibril inside the detection zone (yellow in Figure 6B). In the third step, the fibril stays in the detection zone and the current adopts a plateau. Finally, the current quickly increases due to the exit of the fibril outside the nanopore. We notice that the current blockade last several seconds and thus more than one fibrils can be located inside the nanopore at the same time. This is illustrated in Figure SI-13 where the current based line is not recovered after the fibre exit. To avoid any confusion, we did not take into account such event in the analysis. Thus, we have considered in the analysis only the dwell time corresponding to the fibril location inside the detection zone (in blue Figure 6B). In Figure 7A, the $\Delta I_{max}/I_0$ vs the dwell time of each recorded event is plotted. First, we observe two populations of current blockade for the sample sonicated 60 s. The larger one centred about 0.76 represent ~91% of event could be assigned to the fibril and the smaller one spread from 0.25 to 0.6 (~9 % of events) could be assigned to smaller aggregates (see figure 5C). Conversely, only one population of current blockade was found for the sample sonicated 15 s. The statistical tests show that the two samples sonicated 15 s and 60 s are significantly different (P-value <0.05) (Fig SI-14). However, we notice that the amplitudes of the relative current blockades assigned to the fibrils are similar regardless the sonication time (Figures 6A & SI-13). In order to explain this result, we have to consider the nanopore geometry. Before PEG coating, the diameters of the tip nanopore and the fibrils are close. In this case, the length of the fibrils is not discriminant. For the dwell time, the current blockades have time scales in hundreds milliseconds to 1 second for both samples (Figures 6 A &B). This is two orders of magnitude longer than the dwell time obtained for the non-crowded nanopore

(pore 1 coated with PEG 5 kDa, figure 2). This can be explained by the crowded detection zone by the long PEG chain of 20 kDa . As previously demonstrated in experiments and in MD simulations, such environment increases the dwell time. In addition, we cannot exclude an interaction between fibrils and PEG, also explaining why a high voltage (2 V) is required to observe translocation events. Similarly, to the $\Delta I_{max}/I_0$, the dwell time distributions does not depend on the length of the fibrils. Indeed, there is not significant dwell time distribution for the sample sonicated for 15 s than for the one sonicated for 60 s as confirmed by the p-value >> 0.05 (See Figure 7B).

We also observe trapping events where a fibril blocks the nanopore for a long time preventing the translocation of other fibrils (Figure 6C). In that case, a fibril is blocked inside the nanopore and cannot fully translocate nor go back due to the high electrophoretic force. The trapping events show numerous fluctuations that can be assigned to different orientation of the fibrils inside the nanopore. However, by applying a voltage of -3 V, the nanopore can be reopened due to the removal of the trapped fibril. To characterize trapping events, we compare the power spectrum density (PSD) between the free- and fibril-blocked-nanopore. An increase of PSD at low frequency is observed when the fibril is trapped (Figure SI-15).

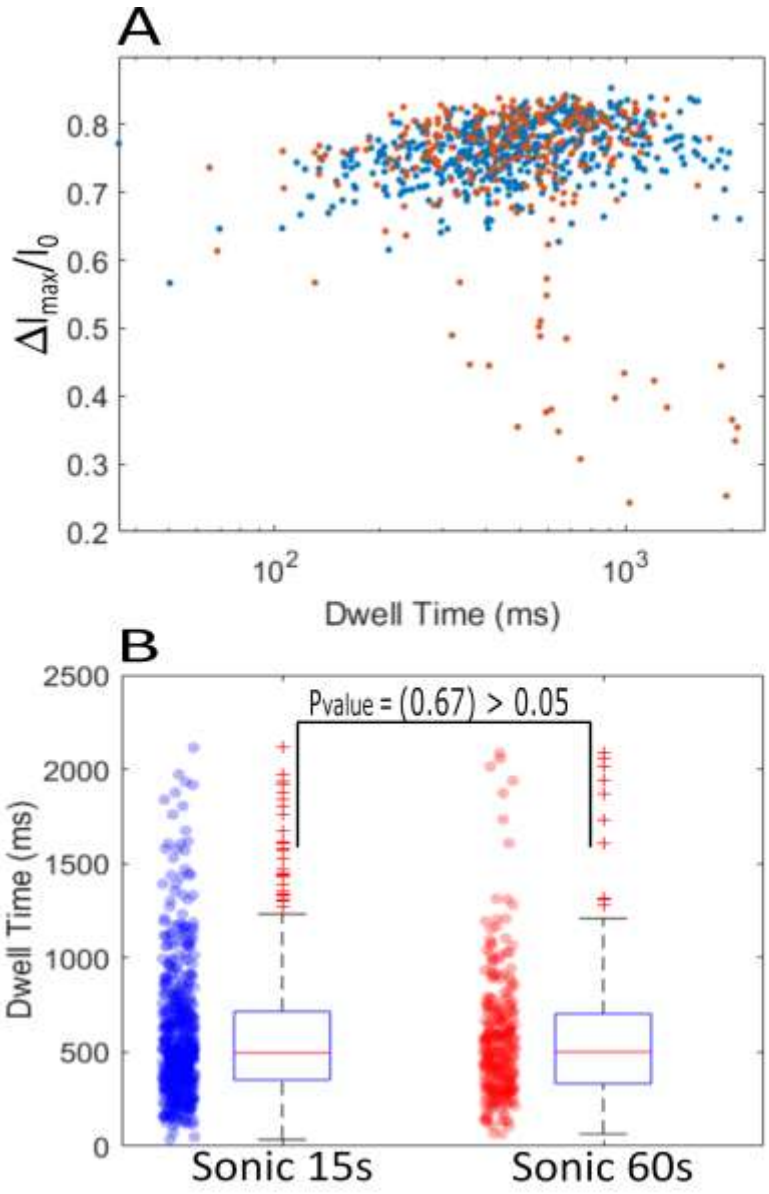

Figure 7 : A) Scatter plot representing the $\Delta I_{max}/I_0$ versus the dwell time for the sample sonicated 15 s (blue, n = 561) and 60 s (red, n = 268). B) Box plot representing the differences of dwell time for the samples sonicated 15 s and 60 s (p-value = 0.67).

To better understand the interactions between the protein and the nanopore during the translocation process, we computed pair interaction energies between the amyloid and the solvent (ion and water) in all the simulations. In Table SI-3 are summarized the averages

values of the energies during the simulation time considering the protein centre of mass is located inside or outside the nanopore. We notice only minor modifications of ion pair energy between solvent and the amyloid inside or outside the nanopore. Water interactions appear to be slightly lowered when the amyloid is located inside the nanopore, while still being comprised in our error bars. Interactions of amyloid with PEG and surface cannot be averaged here since the values fluctuate during the translocation process whether the protein adsorbed to the surface. As observed in Figure SI-16, PEG interactions with the amyloid depends on both the amyloid size and the PEG density. In the low PEG density , we observe for 2NAO a progressive decrease of the pair energies while the amyloid enters in the pore. Then it reaches a plateau about -120 kcal mol^{-1} before returning to 0 as soon as the protein leaves the nanopore. We observe the same trend with 5OQV. However, part of a PEG molecule is still adsorbed on the amyloid even after it left the pore. For the high density PEG, we notice stronger interactions with the amyloid, up to -500 kcal mol^{-1} for 2NAO and -800 kcal mol^{-1} for 5OQV. This is explained by the increase of the number of PEG around the amyloid increases. This is consistent with the slowing down the progression of the amyloid through the pore as shown in Table 1. We cannot establish with precision the lowest pair energy level with the PEG since the curve has not reached their equilibrium. Surface interaction is found to be lower for the high density of PEG, as the latter hide the nanopore surface (Figure SI-17). For the low density of PEG, we observe strong interaction for 5OQV reaching -500 kcal mol^{-1} due to the adsorption of amyloid onto the nanopore surface from 18 to 44 nanoseconds in our simulation. To sum up, our simulation shows that the protein interacts more with the solvent than with the other PEG, and surface. In addition, the protein/solvent interactions do not depend on the PEG density.

However, the amyloid/PEG and amyloid/surface interactions cannot be neglected since represent 1 to 5 % of the interaction with the solvent. This suggests that the amyloid/PEG interaction appears to be the main modified values during the diffusion of the fibrils.

4. Conclusion

In summary, we report detection of Aβ42 fibrillar samples with different length distributions by tuning the shape of track-etched nanopores and PEG functionalization. Our finding that adding EGCG during Aβ42 amyloid formation leads to a different fibril morphotype with an altered fibril length and fragmentation stability is conceptually attractive, and was used here for our nanopore detection strategy to characterize various well-defined fibril populations.

First we found that conical nanopores coated with PEG 5 kDa allow a good discrimination of the fibril size by using $\Delta I_{max}/I_0$. We then demonstrate that the bullet shape nanopore enhances the amplitude of the current by a factor of 3. In addition, the dwell time increases by one order of magnitude. Therefore, we show that by exploiting both these parameters, the $\Delta I_{max}/I_0$ and the dwell time, fibril size can be well discerned. The use of conical nanopores with a tip aperture crowded with large PEG revealed enhanced relative current blockades upon fibril translocation, with no significant differences on both the $\Delta I_{max}/I_0$ and the dwell time between two different-sized fibril samples. Using MD simulations, we then confirmed strong interactions of the fibrils with the PEG functionalization of the conical nanopore, reflected by a larger dwell time.

We demonstrate here in this work that the track-etched nanopore allows to detect and discriminate of fibrils. Indeed, we can control crowding and tune the geometry of the

nanopore by PEG functionalization. Thus, it becomes possible to enhance the amplitude of relative current blockade and/or the dwell time. Considering that, such approach opens the way for further investigation of the different species involved in the amyloidogenesis pathway.

Acknowledgments

This work was founded by Agence Nationale de la Recherche (ANR-19-CE42-0006, NanoOligo). Single tracks have been produced in GANIL (Caen, France) in the framework of an EMIR project. Calculations were performed at the supercomputer regional facility Mesocentre of the University of Franche-Comté with the assistance of K. Mazouzi. This work was also granted access to the HPC resources of IDRIS, Jean Zay supercomputer, under the allocation 2019 - DARI A0070711074 made by GENCI. Finally, part of this work was performed using computing resources of CRIANN (Normandy, France).

References

(1) Chiti, F.; Dobson, C. M. Protein Misfolding, Amyloid Formation, and Human Disease: A Summary of Progress Over the Last Decade. *Annual review of biochemistry* **2017**, *86*, 27–68. DOI: 10.1146/annurev-biochem-061516-045115.

(2) Kelly, J. W. Towards an understanding of amyloidogenesis. *Nature structural biology* **2002**, *9* (5), 323–325. DOI: 10.1038/nsb0502-323.

(3) Soto, C.; Pritzkow, S. Protein misfolding, aggregation, and conformational strains in neurodegenerative diseases. *Nature neuroscience* **2018**, *21* (10), 1332–1340. DOI: 10.1038/s41593-018-0235-9.

(4) Ke, P. C.; Zhou, R.; Serpell, L. C.; Riek, R.; Knowles, T. P. J.; Lashuel, H. A.; Gazit, E.; Hamley, I. W.; Davis, T. P.; Fändrich, M.; Otzen, D. E.; Chapman, M. R.; Dobson, C. M.; Eisenberg, D. S.; Mezzenga, R. Half a century of amyloids: past, present and future. *Chemical Society reviews* **2020**, *49* (15), 5473–5509. Published Online: Jul. 7, 2020.

(5) Morris, A. M.; Watzky, M. A.; Finke, R. G. Protein aggregation kinetics, mechanism, and curve-fitting: a review of the literature. *Biochimica et biophysica acta* **2009**, *1794* (3), 375–397. DOI: 10.1016/j.bbapap.2008.10.016. Published Online: Nov. 11, 2008.

(6) Khurana, R.; Ionescu-Zanetti, C.; Pope, M.; Li, J.; Nielson, L.; Ramírez-Alvarado, M.; Regan, L.; Fink, A. L.; Carter, S. A. A General Model for Amyloid Fibril Assembly Based on Morphological Studies Using Atomic Force Microscopy. *Biophysical journal* **2003**, *85* (2), 1135–1144. DOI: 10.1016/S0006-3495(03)74550-0.

(7) Kasianowicz, J. J.; Brandin, E.; Branton, D.; Deamer, D. W. Characterization of individual polynucleotide molecules using a membrane channel. *PNAS* **1996**, *93* (24), 13770–13773. DOI: 10.1073/pnas.93.24.13770.

(8) Luo, L.; German, S. R.; Lan, W.-J.; Holden, D. A.; Mega, T. L.; White, H. S. Resistive-pulse analysis of nanoparticles. *Annual review of analytical chemistry (Palo Alto, Calif.)* **2014**, *7*, 513–535. DOI: 10.1146/annurev-anchem-071213-020107. Published Online: Jun. 2, 2014.

(9) Yusko, E. C.; Prangkio, P.; Sept, D.; Rollings, R. C.; Li, J.; Mayer, M. Single-particle characterization of Aβ oligomers in solution. *ACS nano* **2012**, *6* (7), 5909–5919. DOI: 10.1021/nn300542q.

(10) Yusko, E. C.; Johnson, J. M.; Majd, S.; Prangkio, P.; Rollings, R. C.; Li, J.; Yang, J.; Mayer, M. Controlling protein translocation through nanopores with bio-inspired fluid walls. *Nature Nanotech* **2011**, *6* (4), 253–260. DOI: 10.1038/nnano.2011.12.

(11) Ouldali, H.; Sarthak, K.; Ensslen, T.; Piguet, F.; Manivet, P.; Pelta, J.; Behrends, J. C.; Aksimentiev, A.; Oukhaled, A. Electrical recognition of the twenty proteinogenic amino acids using an aerolysin nanopore. *Nat Biotechnol* **2020**, *38* (2), 176–181. DOI: 10.1038/s41587-019-0345-2.

(12) Wang, H.-Y.; Ying, Y.-L.; Li, Y.; Kraatz, H.-B.; Long, Y.-T. Nanopore analysis of β-amyloid peptide aggregation transition induced by small molecules. *Analytical chemistry* **2011**, *83* (5), 1746–1752. DOI: 10.1021/ac1029874.

(13) Hu, Y.-X.; Ying, Y.-L.; Gu, Z.; Cao, C.; Yan, B.-Y.; Wang, H.-F.; Long, Y.-T. Single molecule study of initial structural features on the amyloidosis process. *Chemical communications (Cambridge, England)* **2016**, *52* (32), 5542–5545. DOI: 10.1039/c6cc01292b.

(14) Yu, R.-J.; Lu, S.-M.; Xu, S.-W.; Li, Y.-J.; Xu, Q.; Ying, Y.-L.; Long, Y.-T. Single molecule sensing of amyloid-β aggregation by confined glass nanopores. *Chem. Sci.* **2019**, *10* (46), 10728–10732. DOI: 10.1039/C9SC03260F.

(15) Lepoitevin, M.; Ma, T.; Bechelany, M.; Janot, J.-M.; Balme, S. Functionalization of single solid state nanopores to mimic biological ion channels: A review. *Advances in colloid and interface science* **2017**, *250*, 195–213. DOI: 10.1016/j.cis.2017.09.001.

(16) Arima, A.; Tsutsui, M.; Washio, T.; Baba, Y.; Kawai, T. Solid-State Nanopore Platform Integrated with Machine Learning for Digital Diagnosis of Virus Infection. *Analytical chemistry* **2021**, *93* (1), 215–227. DOI: 10.1021/acs.analchem.0c04353. Published Online: Nov. 30, 2020.

(17) Oukhaled, A.; Cressiot, B.; Bacri, L.; Pastoriza-Gallego, M.; Betton, J.-M.; Bourhis, E.; Jede, R.; Gierak, J.; Auvray, L.; Pelta, J. Dynamics of completely unfolded and native proteins through solid-state nanopores as a function of electric driving force. *ACS nano* **2011**, *5* (5), 3628–3638. DOI: 10.1021/nn1034795.

(18) Waduge, P.; Hu, R.; Bandarkar, P.; Yamazaki, H.; Cressiot, B.; Zhao, Q.; Whitford, P. C.; Wanunu, M. Nanopore-Based Measurements of Protein Size, Fluctuations, and Conformational Changes. *ACS nano* **2017**, *11* (6), 5706–5716. DOI: 10.1021/acsnano.7b01212.

(19) Kowalczyk, S. W.; Dekker, C. Measurement of the docking time of a DNA molecule onto a solid-state nanopore. *Nano Lett.* **2012**, *12* (8), 4159–4163. DOI: 10.1021/nl301719a.

(20) Coglitore, D.; Giamblanco, N.; Kizalaité, A.; Coulon, P. E.; Charlot, B.; Janot, J.-M.; Balme, S. Unexpected Hard Protein Behavior of BSA on Gold Nanoparticle Caused by Resveratrol. *Langmuir : the ACS journal of surfaces and colloids* **2018**, *34* (30), 8866–8874. DOI: 10.1021/acs.langmuir.8b01365.

(21) Houghtaling, J.; List, J.; Mayer, M. Nanopore-Based, Rapid Characterization of Individual Amyloid Particles in Solution: Concepts, Challenges, and Prospects. *Small (Weinheim an der Bergstrasse, Germany)* **2018**, *14* (46), e1802412. DOI: 10.1002/smll.201802412.

(22) Giamblanco, N.; Coglitore, D.; Janot, J.-M.; Coulon, P. E.; Charlot, B.; Balme, S. Detection of protein aggregate morphology through single antifouling nanopore. *Sensors and Actuators B: Chemical* **2018**, *260*, 736–745. DOI: 10.1016/j.snb.2018.01.094.

(23) Balme, S.; Coulon, P. E.; Lepoitevin, M.; Charlot, B.; Yandrapalli, N.; Favard, C.; Muriaux, D.; Bechelany, M.; Janot, J.-M. Influence of Adsorption on Proteins and Amyloid Detection by Silicon Nitride Nanopore. *Langmuir : the ACS journal of surfaces and colloids* **2016**, *32* (35), 8916–8925. DOI: 10.1021/acs.langmuir.6b02048.

(24) Yusko, E. C.; Bruhn, B. R.; Eggenberger, O. M.; Houghtaling, J.; Rollings, R. C.; Walsh, N. C.; Nandivada, S.; Pindrus, M.; Hall, A. R.; Sept, D.; Li, J.; Kalonia, D. S.; Mayer, M. Real-time shape approximation and fingerprinting of single proteins using a nanopore. *Nature Nanotech* **2017**, *12* (4), 360–367. DOI: 10.1038/nnano.2016.267.

(25) Li, X.; Tong, X.; Lu, W.; Yu, D.; Diao, J.; Zhao, Q. Label-free detection of early oligomerization of α-synuclein and its mutants A30P/E46K through solid-state nanopores. *Nanoscale* **2019**, *11* (13), 6480–6488. DOI: 10.1039/C9NR00023B.

(26) Lenhart, B.; Wei, X.; Watson, B.; Wang, X.; Zhang, Z.; Li, C.-z.; Moss, M.; Liu, C. In vitro biosensing of β-Amyloid peptide aggregation dynamics using a biological nanopore. *Sensors and Actuators B: Chemical* **2021**, *338*, 129863. DOI: 10.1016/j.snb.2021.129863.

(27) Ma, T.; Janot, J.-M.; Balme, S. Track-Etched Nanopore/Membrane: From Fundamental to Applications. *Small Methods* **2020**, 2000366. DOI: 10.1002/smtd.202000366.

(28) Giamblanco, N.; Coglitore, D.; Gubbiotti, A.; Ma, T.; Balanzat, E.; Janot, J.-M.; Chinappi, M.; Balme, S. Amyloid Growth, Inhibition, and Real-Time Enzymatic Degradation Revealed with Single Conical Nanopore. *Analytical chemistry* **2018**, *90* (21), 12900–12908. DOI: 10.1021/acs.analchem.8b03523.

(29) Chau, C. C.; Radford, S. E.; Hewitt, E. W.; Actis, P. Macromolecular Crowding Enhances the Detection of DNA and Proteins by a Solid-State Nanopore. *Nano letters* **2020**, *20* (7), 5553–5561. DOI: 10.1021/acs.nanolett.0c02246.

(30) Ma, T.; Arroyo, N.; Marc Janot, J.; Picaud, F.; Balme, S. Conformation of Polyethylene Glycol inside Confined Space: Simulation and Experimental Approaches. *Nanomaterials (Basel, Switzerland)* **2021**, *11* (1), 244. DOI: 10.3390/nano11010244.

(31) Ma, T.; Balanzat, E.; Janot, J.-M.; Balme, S. Single conical track-etched nanopore for a free-label detection of OSCS contaminants in heparin. *Biosensors & bioelectronics* **2019**, *137*, 207–212. DOI: 10.1016/j.bios.2019.05.005.

(32) Roman, J.; Jarroux, N.; Patriarche, G.; Français, O.; Pelta, J.; Le Pioufle, B.; Bacri, L. Functionalized Solid-State Nanopore Integrated in a Reusable Microfluidic Device for a Better Stability and Nanoparticle Detection. *ACS applied materials & interfaces* **2017**, *9* (48), 41634–41640. DOI: 10.1021/acsami.7b14717.

(33) Giamblanco, N.; Fichou, Y.; Janot, J.-M.; Balanzat, E.; Han, S.; Balme, S. Mechanisms of Heparin-Induced Tau Aggregation Revealed by a Single Nanopore. *ACS sensors* **2020**, *5* (4), 1158–1167. DOI: 10.1021/acssensors.0c00193.

(34) Chau, C. C.; Hewitt, E. W.; Actis, P. The role of macromolecular crowding in single-entity electrochemistry: Friend or foe? *Current Opinion in Electrochemistry* **2021**, *25*, 100654. DOI: 10.1016/j.coelec.2020.100654.

(35) Lepoitevin, M.; Jamilloux, B.; Bechelany, M.; Balanzat, E.; Janot, J.-M.; Balme, S. Fast and reversible functionalization of a single nanopore based on layer-by-layer polyelectrolyte self-assembly for tuning current rectification and designing sensors. *RSC Adv.* **2016**, *6* (38), 32228–32233. DOI: 10.1039/C6RA03698H.

(36) Zhao, Y.; Janot, J.-M.; Balanzat, E.; Balme, S. Mimicking pH-Gated Ionic Channels by Polyelectrolyte Complex Confinement Inside a Single Nanopore. *Langmuir : the ACS journal of surfaces and colloids* **2017**, *33* (14), 3484–3490. DOI: 10.1021/acs.langmuir.7b00377.

(37) Apel, P.Y.; Blonskaya, I. V.; Dmitriev, S. N.; Orelovich, O. L.; Sartowska, B. A. Ion track symmetric and asymmetric nanopores in polyethylene terephthalate foils for versatile applications. *Nuclear Instruments and Methods in Physics Research Section B: Beam Interactions with Materials and Atoms* **2015**, *365*, 409–413. DOI: 10.1016/j.nimb.2015.07.016.

(38) Apel, P. Y.; Blonskaya, I. V.; Orelovitch, O. L.; Ramirez, P.; Sartowska, B. A. Effect of nanopore geometry on ion current rectification. *Nanotechnology* **2011**, *22* (17), 175302. DOI: 10.1088/0957-4484/22/17/175302.

(39) Phillips, J. C.; Braun, R.; Wang, W.; Gumbart, J.; Tajkhorshid, E.; Villa, E.; Chipot, C.; Skeel, R. D.; Kalé, L.; Schulten, K. Scalable molecular dynamics with NAMD. *Journal of computational chemistry* **2005**, *26* (16), 1781–1802. DOI: 10.1002/jcc.20289.

(40) Best, R. B.; Zhu, X.; Shim, J.; Lopes, P. E. M.; Mittal, J.; Feig, M.; MacKerell, A. D. Optimization of the additive CHARMM all-atom protein force field targeting improved sampling of the backbone ϕ, ψ and side-chain χ(1) and χ(2) dihedral angles. *Journal of Chemical Theory and Computation* **2012**, *8* (9), 3257–3273. DOI: 10.1021/ct300400x.

(41) Geyer, T. Many-particle Brownian and Langevin Dynamics Simulations with the Brownmove package. *BMC biophysics* **2011**, *4*, 7. DOI: 10.1186/2046-1682-4-7. Published Online: Apr. 13, 2011.

(42) Feller, S. E.; Zhang, Y.; Pastor, R. W.; Brooks, B. R. Constant pressure molecular dynamics simulation: The Langevin piston method. *The Journal of Chemical Physics* **1995**, *103* (11), 4613–4621. DOI: 10.1063/1.470648.

(43) Darden, T.; York, D.; Pedersen, L. Particle mesh Ewald: An N ·log(N) method for Ewald sums in large systems. *The Journal of Chemical Physics* **1993**, *98* (12), 10089–10092. DOI: 10.1063/1.464397.

(44) Arroyo, N.; Balme, S.; Picaud, F. Impact of surface state on polyethylene glycol conformation confined inside a nanopore. *The Journal of Chemical Physics* **2021**, *154* (10), 104901. DOI: 10.1063/5.0040170.

(45) Gremer, L.; Schölzel, D.; Schenk, C.; Reinartz, E.; Labahn, J.; Ravelli, R. B. G.; Tusche, M.; Lopez-Iglesias, C.; Hoyer, W.; Heise, H.; Willbold, D.; Schröder, G. F. Fibril structure of amyloid-β(1-42) by cryo-electron microscopy. *Science (New York, N.Y.)* **2017**, *358* (6359), 116–119. DOI: 10.1126/science.aao2825.

(46) Giamblanco, N.; Janot, J.-M.; Gubbiotti, A.; Chinappi, M.; Balme, S. Characterization of Food Amyloid Protein Digestion by Conical Nanopore. *Small Methods* **2020**, *9*, 1900703. DOI: 10.1002/smtd.201900703.

(47) Lan, W.-J.; Holden, D. A.; Zhang, B.; White, H. S. Nanoparticle transport in conical-shaped nanopores. *Analytical chemistry* **2011**, *83* (10), 3840–3847. DOI: 10.1021/ac200312n. Published Online: Apr. 25, 2011.